Sol-gel enhanced mesoporous Cu-Ce-Zr catalyst for toluene oxidation

Running Kang, Xiaolin Wei, Huixin Li, Feng Bin, Ruozhu Zhao, Qinglan Hao & Baojuan Dou

Taylor & Francis
Taylor & Francis Group

Check for updates

Sol-gel enhanced mesoporous Cu-Ce-Zr catalyst for toluene oxidation

Running Kang[a,b], Xiaolin Wei[a,c], Huixin Li[a,c], Feng Bin[a], Ruozhu Zhao[d], Qinglan Hao[d], and Baojuan Dou[d]

[a]State Key Laboratory of High-Temperature Gas Dynamics, Institute of Mechanics, Chinese Academy of Sciences, Beijing, PR China; [b]College of Metallurgy and Energy, North China University of Science and Technology, Tangshan, PR China; [c]School of Engineering Science, University of Chinese Academy of Sciences, Beijing, PR China; [d]College of Environmental Sciences, Tianjin University of Science & Technology, Tianjin, PR China

ABSTRACT

The bulk-phase Cu-Ce-Zr catalyst BP-gel was prepared by the sol-gel method and investigated for the oxidation of toluene in a fixed-bed reactor. For comparison, other bulk-phase catalysts (thermal decomposition (BP-td), solid-state reaction (BP-sr)) and supported catalysts (incipient wetness impregnation (S-iwi), saturated impregnation (S-si)) were tested. The results showed that the catalytic activities were in the following order: BP-gel>S-si>S-iwi>BP-td>BP-sr. The BP-gel catalyst, which has a mesoporous structure, is beneficial for the mass transfer of reactant molecules. The thermal stability of the BP-gel catalyst was improved by the introduction of ZrO_2. Bulk CuO in the catalysts reduced their activity because the synergetic effect between CuO and CeO_2 decreased. The low-temperature reducibility, large pore sizes, rich oxygen vacancies, and active oxygen species contributed to the highest activity of the BP-gel, with a T_{90} as low as 219°C, and no deactivation was observed during the 72 h stability test at the set temperature.

Introduction

Currently, volatile organic compounds (VOCs) from natural and industrial sources are considered a main cause of current serious environmental problems. Their toxic nature leads to serious air pollution, such as photochemical smog, haze, and the production of ground-level ozone (He et al., 2015a; He et al., 2014; Kuo et al., 2014). Hence, environmental air quality standards have been greatly increased and strictly enforced, which has led to much attention to the development of efficient methods for VOC abatement (Gutiérrez-Ortiz et al., 2006).

Catalytic oxidation is emerging as an environmentally friendly technique for the degradation of VOCs (Tang et al., 2015a, Wang et al., 2015a). Typical catalysts employed for VOC oxidation are multi-component metal oxides, since they have a lower cost than noble metal catalysts, although the former exhibit activity at moderate temperature (Li et al., 2016, Lu et al., 2015). It is well known that the structure–activity

relationship of metal oxides is determined by traditional preparation methods, such as co-precipitation, impregnation, and hydrothermal synthesis, but unfortunately, such bulk-phase catalysts, which are obtained with small pore size, always limit the enhancement of their activity (Hu et al., 2009). By contrast, the sol-gel method can be successfully employed to synthesize metal oxides with relatively broad pore size distributions and large pore volumes. In this case, the unique mesoporous structure is highly beneficial for the migration and diffusion of reactant molecules during reaction. Previously, a Mn-Ce composite oxide with a mesoporous structure, prepared by the sol-gel method, was successfully applied to benzene oxidation. Although the low-temperature reducibility, broad pore size distribution and rich adsorbed surface oxygen species greatly contribute to the activity toward benzene oxidation, the stability is still unsatisfactory, as the activity decreases from 100% to 92% after 12 h at 275°C (Tang et al., 2015b).

Mixed metal oxide catalysts containing copper, cerium and zirconium have attracted great interest in low-temperature VOC oxidation (Bin et al., 2014). In these catalysts, CuO is considered to be the active component due to their excellent reducibility (Zhang et al., 2015a). CeO_2 not only promotes the dispersion of active copper species but provides a large oxygen storage-release capacity owing to the Ce^{4+}-Ce^{3+} redox couple in the cubic fluorite structure (Zhou et al., 2014). Although ZrO_2 cannot contribute to the catalytic activity directly, zirconium entering the CeO_2 lattice has a strong effect on its thermal stability and thus provides the possibility to improve the catalytic performance through the formation of a Ce-Zr solid solution (Moretti et al., 2017; Riva et al., 2009).

In this study, a bulk-phase $CuCe_{0.75}Zr_{0.25}O_y$ catalyst with a mesoporous structure and highly dispersed CuO was synthesized using the sol-gel method. Here, the ratio of Cu:Ce:Zr was set at 1:0.75:0.25 based on our previous study, where $CuCe_{0.75}Zr_{0.25}O_y$ mixed oxides formed on ZSM-5 substrates showed higher activities for the catalytic removal of ethyl acetate than other ratios because the copper–ceria synergism improves the excellent redox capability and the ceria–zirconium solid solution has a good oxygen storage capacity under these conditions (Dou et al., 2011). However, the adsorption, desorption and diffusion of VOCs were restricted by the microporous ZSM-5, increasing the possibility of secondary reactions and coke formation. For comparison, bulk-phase $CuCe_{0.75}Zr_{0.25}O_y$ catalysts were synthesized by typical methods, e.g., thermal decomposition and solid-state reaction methods, and supported $CuCe_{0.75}Zr_{0.25}O_y$/H-ZSM-5 catalysts with the same composition of $CuCe_{0.75}Zr_{0.25}O_y$ were also prepared by incipient wetness impregnation and saturated impregnation.

The aim of this study is to determine the influence of the pore size of the bulk-phase CuO-CeO_2-ZrO_2 catalysts on the oxygen vacancies in the catalysts, the migration and diffusion of VOCs, the catalytic activity, and the stability. The catalytic activity was evaluated toward the oxidation of toluene, which is a typical aromatic hydrocarbon extensively applied in industrial processes. Combined with characterization techniques such as Brunauer-Emmett-Teller (BET) analysis, X-ray diffraction (XRD), temperature-programmed desorption of oxygen (O_2-TPD), temperature-programmed desorption of ammonia (NH_3-TPD), and temperature-programmed hydrogen reduction (H_2-TPR), the relationship between the physico-chemical properties, the reaction mechanism and the activity for toluene oxidation over the catalysts was investigated in detail.

Experimental

Catalyst preparation

$Cu(NO_3)_2 \cdot 3H_2O$, $Ce(NO_3)_3 \cdot 6H_2O$ and $Zr(NO_3)_4 \cdot 5H_2O$ (A.R.) were purchased from Jiangtian Co., Ltd., Tianjin, P. R. China. Deionized water was used in all experimental processes. H-ZSM-5 with an atomic Si/Al ratio of 25 was supplied by Nankai University, Tianjin, P. R. China.

Bulk-phase $cuce_{0.75}zr_{0.25}o_y$ catalyst preparation

Bulk-phase $CuCe_{0.75}Zr_{0.25}O_y$ catalysts were prepared by three methods, namely, sol-gel, thermal decomposition and solid-state reaction. The molar ratio of $Cu/(Ce+Zr)$ in the $CuCe_{0.75}Zr_{0.25}O_y$ catalysts was controlled at 1:1. The molar content of the CuO, CeO_2 and ZrO_2 in prepared catalysts was also detected by XRF.

(1) Sol-gel method (BP-gel)

$Cu(NO_3)_2 \cdot 3H_2O$, $Ce(NO_3)_3 \cdot 6H_2O$ and $Zr(NO_3)_4 \cdot 5H_2O$ in a 4:3:1 molar ratio were dissolved in 70 mL of ethanol at 80°C. Then, 0.24 mol/L of oxalic acid solution was added quickly to the above nitrate solution with stirring until a gel was formed. The gel was continuously stirred and kept at 80°C for 12 h. After aging at room temperature for approximately 48 h, the gel was dried at 80°C for 12 h and calcined at 550°C for another 2 h.

(2) Thermal decomposition method (BP-td)

Appropriate amounts of $Cu(NO_3)_2 \cdot 3H_2O$, $Ce(NO_3)_3 \cdot 6H_2O$ and $Zr(NO_3)_4 \cdot 5H_2O$ were dissolved in 350 mL of deionized water at room temperature. The mixed solution was first evaporated to dryness at 80°C, and then, the mixture was further kept at 105°C for 24 h and calcined at 550°C for 2 h.

(3) Solid-state reaction (BP-sr)

$Cu(NO_3)_2 \cdot 3H_2O$, $Ce(NO_3)_3 \cdot 6H_2O$ and $Zr(NO_3)_4 \cdot 5H_2O$ in the desired molar ratio were first milled using mechanical mixing for 10 min, and then, the mixed sample was calcined in air at 550°C for 2 h before use.

Supported $Cuce_{0.75}Zr_{0.25}O_y$/H-ZSM-5 catalyst preparation

Supported $CuCe_{0.75}Zr_{0.25}O_y$/H-ZSM-5 catalysts were prepared by saturated impregnation and incipient impregnation. The copper contents of the $CuCe_{0.75}Zr_{0.25}O_y$/H-ZSM-5 catalysts were fixed at 4 wt%, and the molar ratio of $Cu/(Ce+Zr)$ was 1:1.

(1) Saturated impregnation (S-si)

The synthesis of the supported catalyst prepared by saturated impregnation has been provided previously (Dou et al., 2011). In brief, appropriate amounts of copper acetate, zirconium, and cerium nitrate were dissolved in deionized water and mixed with 20 g

H-ZSM-5 powder at the temperature of 70 °C until the water evaporated. Then, the resulting precursor was dried at 105°C for 24 h in air and calcined at 550°C for 4 h.

(2) Incipient impregnation (S-iwi)

Desired amounts of copper acetate, zirconium, and cerium nitrate were dissolved in 25 mL of deionized water. Then, 20 g of H-ZSM-5 was added to the solution and stirred. The resulting mixture was kept at 30°C for 12 h. Finally, the precursor was dried at 105°C for 12 h and calcined at 550°C for 4 h under ambient atmosphere.

Catalyst characterization

N_2 adsorption-desorption isotherms were collected at −196°C using an Autosorb-Iq-MP instrument (Quantachrome). The sample was degassed at 300°C for more than 4 h before measurement. The specific surface area of the samples was calculated following the Brunauer–Emmett–Teller (BET) method. The average pore size was obtained by the Barrett–Joyner–Halenda (BJH) method and non-local density functional theory (NLDFT) modeling. The X-ray diffraction (XRD) analysis was performed on an XD-3-automatic (PERSEE) with Cu Kα radiation. The patterns were collected over a 2θ range of 5° to 80° with a step size of 0.02° at a scanning rate of 4°/min. Temperature-programmed reduction (TPR) experiments were carried out using a PCA-140 instrument (Bolider) equipped with a thermal conductivity detector (TCD). First, 200 mg of sample was pretreated in an Ar stream at 500°C for 1 h at a rate of 20°C/min and then cooled to room temperature. After that, a reduction gas of 5% H_2/Ar was introduced at a flow rate of 50 mL/min. The sample was heated from room temperature to 800°C at a heating rate of 10 °C/min. The temperature-programmed desorption of oxygen (O_2-TPD) was recorded on the same PCA-140 instrument. For this, 200 mg of fresh catalyst was used, and then, O_2 was adsorbed at 550°C for 30 min, cooled to 30°C, and then exposed to Ar (50 mL/min); the reactor was heated at a rate of 10°C/min until reaching 950°C. Temperature-programmed desorption of ammonia (NH_3-TPD) experiments were used to measure the surface acidity of the catalysts. First, 200 mg of sample was pretreated in an Ar stream (50 mL/min) at 500°C for 1 h at a rate of 20°C/min and then cooled to room temperature. Second, the catalyst was exposed to a flow of 5% NH_3/Ar (50 mL/min) at 100°C for 30 min to reach saturation. Finally, the NH_3 desorption profile was recorded from 100°C to 800°C under Ar stream flow (50 mL/min, at a heating rate of 10°C/min).

## Catalytic activity measurement

Toluene was selected as a probe pollutant to examine the removal effectiveness of the catalysts, and the toluene oxidation reaction was performed in a fixed-bed reactor, in which approximately 0.8 g of catalyst (20–40 mesh) was loaded. The reaction temperature was monitored by a thermocouple located inside the catalyst bed. The reaction feed is 1500 ppm of toluene in dry air with a total gas flow of 400 mL/min and space velocity (SV) of 24,000 h^{-1}. The reactor was heated from room temperature to 110°C at a heating rate of 1°C/min in flowing air and held at this temperature for 30 min before catalytic activity testing. The compositions at the inlet and outlet of the reactor were analyzed using

a gas chromatograph (GC-7900, Shanghai Tianmei Co., China) with a flame ionization detector (FID, HP-5) for the quantitative analysis of toluene, and a TCD (TDX-01) was used for the quantitative analysis of CO_2. The conversion of toluene was calculated based on the concentration differences between the inlet and outlet gases. The selectivity toward CO_2 was calculated as a percentage of the outlet concentration of CO_2 to the total content of toluene converted to CO_2.

Results and discussion

Catalyst textural properties

The N_2 adsorption-desorption isotherms and corresponding pore size distribution curves of the bulk-phase $CuCe_{0.75}Zr_{0.25}O_y$ catalysts and supported $CuCe_{0.75}Zr_{0.25}O_y$/H-ZSM-5 catalysts are shown in Figure 1. It is clearly seen from Figure 1 (a) that the supported S-iwi and S-si catalysts exhibit a representative type I isotherm according to the IUPAC classification. There are two curves with the same color and markers for each catalyst, which correspond to the N_2 adsorption-desorption isotherm. The pore size distributions can be calculated according to the hysteresis loop formed by the two curves for each catalyst. When the relative pressure is less than 0.02, the increase in the adsorbed amount indicates that the volume is filled with micropores belonging to the H-ZSM-5 structure (Ge et al., 2015). By contrast, BP-td and BP-sr show type IV isotherms with a H3-type hysteresis loop, suggesting the presence of mesopores. The amount of adsorbed N_2 increases significantly when the relative pressure is close to 1, which is due to volume filling of the interparticle spaces (He et al., 2015a). With respect to BP-gel, typical type IV adsorption isotherms and a steep capillary condensation step with H_2-type hysteresis loop are clearly observed in Figure 1 (a), indicating the formation of worm-like mesopores in the catalyst. It is further demonstrated
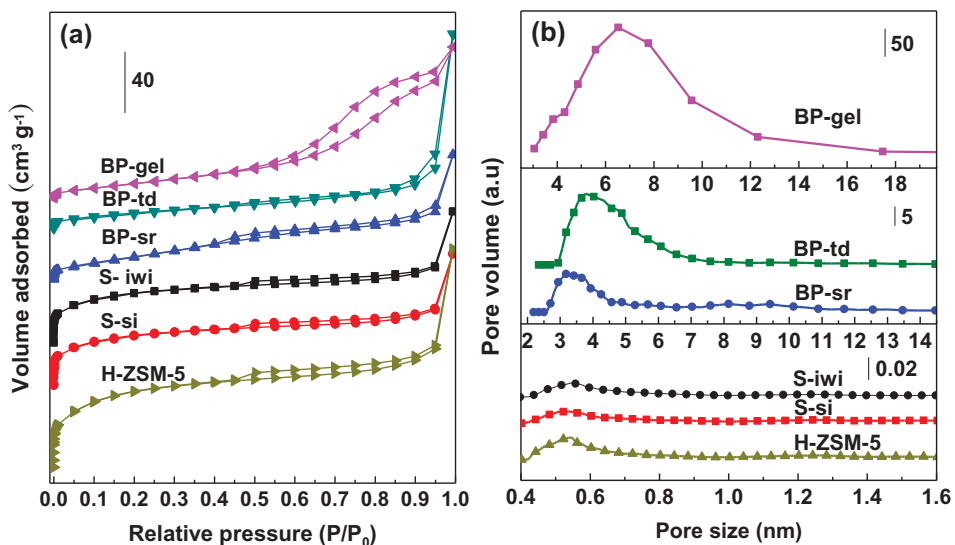
Figure 1. N_2 adsorption and desorption isotherms (a) and pore size distributions (b) of $CuCe_{0.75}Zr_{0.25}O_y$ and $CuCe_{0.75}Zr_{0.25}O_y$/H-ZSM-5catalysts.

that mesopores are dominant in the BP-gel by comparing the pore size distributions in Figure 1 (b), while the pore size distribution curves of S-iwi and S-si present one single narrow peak in the microporous range at ca. 0.4–0.65 nm.
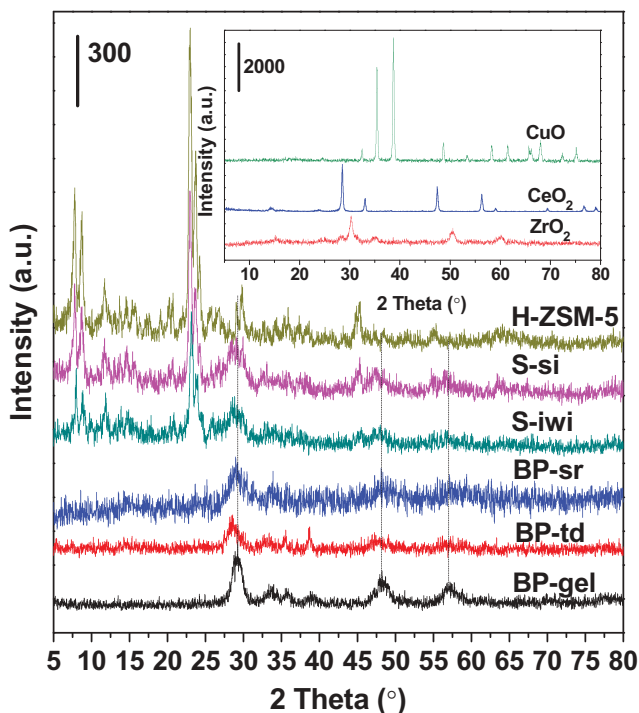
Table 1 displays the BET surface area, pore volume, and mean pore diameter of the catalysts. The pore sizes of S-iwi (0.37 nm) and S-si (0.53 nm) are much lower than those of BP-gel (6.52 nm), BP-td (3.54 nm), and BP-sr (3.78 nm). Furthermore, the S_{BET} of the supported catalysts (295–339 m^2/g) are observed to be much higher than those of the bulk-phase catalysts (44–62 m^2/g) owing to the high surface area of the H-ZSM-5 support. The pore volumes are determined to follow the sequence S-si>S-iwi>BP-td>BP-gel>BP-sr. The BET surface area and total pore volume of the supported S-si and S-iwi catalysts are observed to be lower than those of H-ZSM-5 due to the presence of Cu-Ce-Zr ternary oxides in the pores of H-ZSM-5 (Chen et al., 2014).

Crystal structure of the catalysts

Figure 2 presents the XRD patterns of the catalysts, and the lattice parameters of the BP-td, BP-gel and BP-sr catalysts are summarized in Table 1. It is clearly seen that the characteristic diffraction peaks are quite different between the bulk-phase catalysts and the supported catalysts. For the supported catalysts S-si and S-iwi, only the characteristic diffraction peaks of H-ZSM-5 are observed, which is indicative of copper, cerium, and zirconium oxides existing in the nanometer range and their uniform distribution on the H-ZSM-5 surface (Bin et al., 2014), while the supported catalysts maintain their microstructures. For the bulk-phase catalysts of BP-td, BP-gel and BP-sr, the characteristic diffraction peaks of CeO$_2$ are observed to be weaker and broader than those of pure CeO$_2$. The peak of CeO$_2$ at 2θ = 28.2° is clearly seen to shift to a higher 2θ value, while the peaks of CeO$_2$ at 2θ>60° in all the bulk-phase catalysts disappear. In Table 1, the lattice parameters of the BP-td, BP-gel and BP-sr catalysts decrease slightly compared with those of pure CeO$_2$, suggesting the formation of lattice defects and oxygen vacancies due to Cu^{2+} ion (0.072 nm) and Zr^{4+} ion (0.084 nm) incorporation into the CeO$_2$ lattice. The results are also consistent with previously reported work (Jia et al., 2012; Luo et al., 2007). The presence of lattice defects and oxygen vacancies in the catalyst can greatly contribute to the formation of absorbed oxygen. The active oxygen species resulting from the adsorbed oxygen can subsequently promote the activity of the catalytic oxidation of VOCs (Hu et al., 2009). Furthermore, two weak diffraction peaks corresponding to bulk CuO in the BP-gel and BP-td catalysts are clearly observed, suggesting the presence of CuO species in the aggregation state.

Table 1. Textural properties of CuCe$_{0.75}$Zr$_{0.25}$O$_y$ and CuCe$_{0.75}$Zr$_{0.25}$O$_y$/H-ZSM-5 catalysts.

Samples	Surface area (m^2·g^{-1})	Mean pore size (nm)	Pore volume (cm^3·g^{-1})	Lattice parameters (Å)
BP-gel	59	6.52	0.17	5.368
BP-td	44	3.54	0.19	5.389
BP-sr	62	3.78	0.13	5.407
S-si	339	0.53	0.29	–
S-iwi	295	0.37	0.23	–
H-ZSM-5	501	0.54	0.35	–
CeO$_2$	–	–	–	5.417

Figure 2. XRD patterns of $CuCe_{0.75}Zr_{0.25}O_y$ and $CuCe_{0.75}Zr_{0.25}O_y$/H-ZSM-5 catalysts.

Temperature-programmed hydrogen reduction

The reducibility of different Cu-Ce-Zr catalysts was investigated by H_2-TPR, and the curves and corresponding H_2 consumption are given in Figure 3 and Table 2, respectively. The content of active components in the bulk-phase catalysts is higher than that in the supported catalysts, which is responsible for the high H_2 consumption. In Figure 3, the broad peak of H_2 consumption can be split into approximately four peaks (α, β, γ, and δ). The α peak at approximately 150–200°C is assigned to the well-dispersed copper oxide species strongly interacting with CeO_2 (He et al., 2015b), while the reduction of Cu^{2+} ions in the CeO_2 lattice is responsible for the β peak at approximately 200–250°C (Dou et al., 2011). The γ peak at approximately 250–300°C is due to the reduction of bulk-like CuO (Tang et al., 2015b). The δ peak at above 300°C is probably attributed to the reduction of CeO_2 (He et al., 2014). The broad peak of H_2 consumption for the BP-td catalyst can be split into four peaks (α, β, γ, and δ). In addition, the H_2-TPR profile of the BP-gel catalyst is consistent with that of the BP-td catalyst, but all the peaks are shifted to lower temperatures. Such a phenomenon can be explained by the fact that a strong synergetic interaction between CuO and CeO_2 can improve the mobility of the active oxygen species on the BP-gel catalyst surface, which is favorable for the redox cycle between Cu^{2+}/Cu^+ and Ce^{3+}/Ce^{4+} (Luo et al., 2007). Unlike the BP-gel and BP-td catalysts, three H_2 consumption peaks (α, β, and γ) are examined for the BP-sr catalyst, and the lack of a δ peak results in reduced H_2 consumption (1128 μmol/g). The H_2 consumption of the supported catalysts is lower than that of the bulk-phase catalysts (Table 2) due to a low amount of active component in the supported catalysts. The reduction peaks of the bulk-phase $CuCe_{0.75}Zr_{0.25}O_y$ catalysts and supported
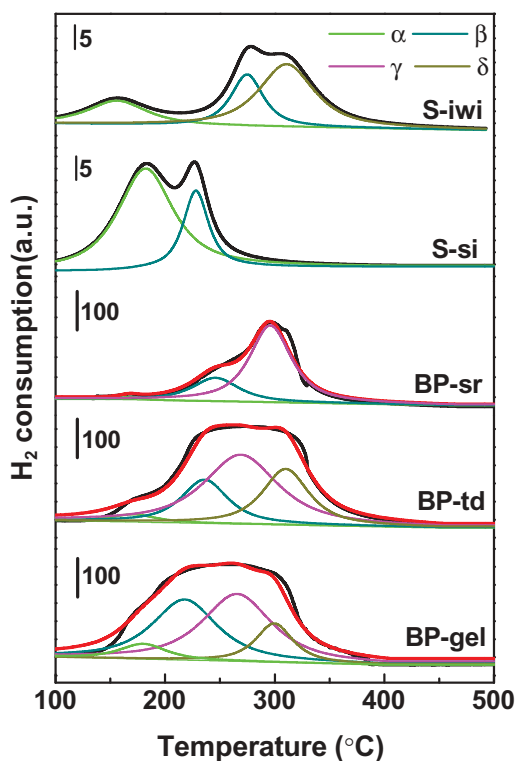
Figure 3. H_2-TPR profiles of $CuCe_{0.75}Zr_{0.25}O_y$ catalysts and $CuCe_{0.75}Zr_{0.25}O_y$/H-ZSM-5 catalysts.

Table 2. H_2 consumption of $CuCe_{0.75}Zr_{0.25}O_y$ and $CuCe_{0.75}Zr_{0.25}O_y$/H-ZSM-5 catalysts.

Samples	H_2 consumption ($\mu mol \cdot g^{-1}$)				
	α peak	β peak	γ peak	δ peak	Total
BP-gel	197	1128	1331	439	3096
BP-td	98	584	1469	741	2892
BP-sr	13	282	833	–	1128
S-si	125	39	–	–	164
S-iwi	33	–	39	72	144

$CuCe_{0.75}Zr_{0.25}O_y$/H-ZSM-5 catalysts shift to lower temperatures compared with the reduction of CuO and CeO_2 (Zhang et al., 2014). The shift toward lower temperatures may be partially caused by Zr^{4+} and Cu^{2+} ions inserting into the CeO_2 lattice, which improves the mobility of the lattice oxygen and successively increases the lattice defects and oxygen vacancies (Zhou et al., 2014). The shift was probably also attributed to strong interactions between CuO and CeO_2 in the Cu-Ce-Zr-O solid solution that weaken the Cu-O and Ce-O chemical bonds (Bin et al., 2014).

Temperature-programmed desorption of ammonia

The NH_3-TPD profiles of H-ZSM-5 and the synthesized catalysts are shown in Figure 4. Obvious differences in the acidity between the bulk-phase catalyst and the supported catalyst
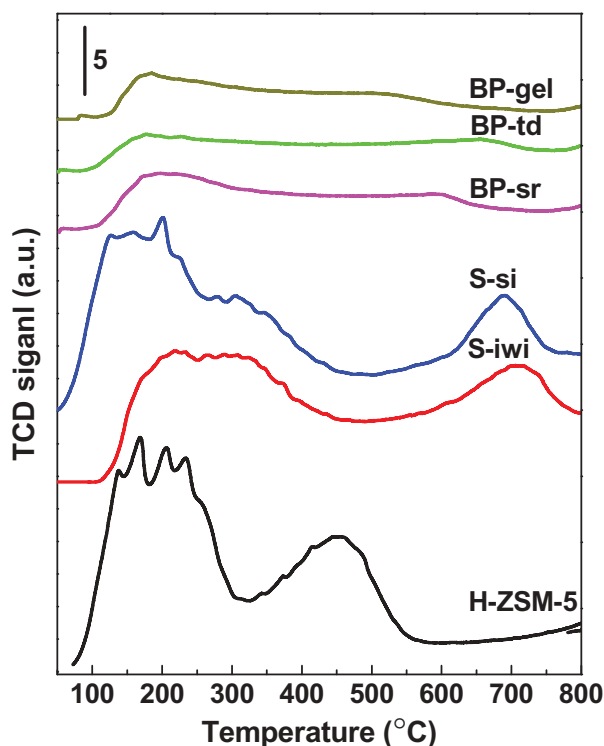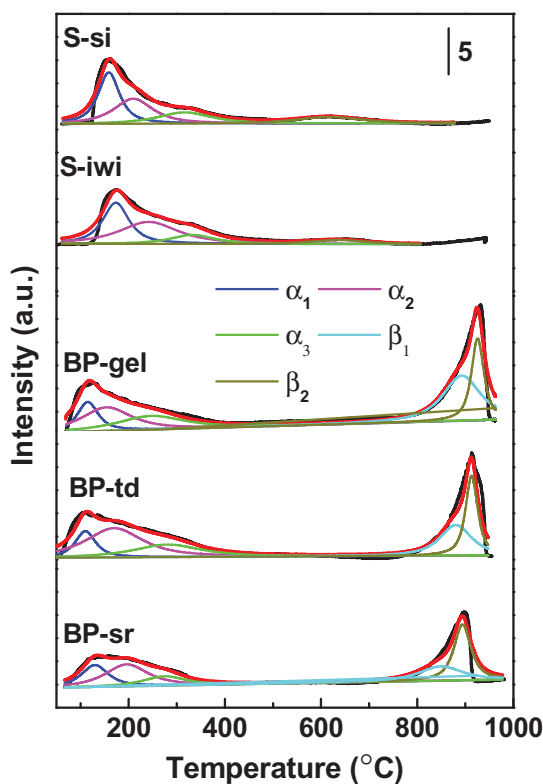
Figure 4. NH$_3$-TPD profiles of CuCe$_{0.75}$Zr$_{0.25}$O$_y$ and CuCe$_{0.75}$Zr$_{0.25}$O$_y$/H-ZSM-5 catalysts.

are clearly observed, suggesting that the catalyst acidity primarily derives from H-ZSM-5. The NH$_3$-TPD desorption peak of H-ZSM-5 exhibits a low-temperature peak caused by the physical adsorption of ammonia bound to Si-OH, and a high-temperature peak is also clearly seen due to NH$_3$ adsorption on the strong acid sites of Si-OH-Al (Dou et al., 2011). As such, the NH$_3$-TPD profiles of the supported catalysts exhibit two peaks corresponding to desorption at the weak acid sites and at the strong acid sites, but their intensities lower are than those of H-ZSM-5. Compared to the NH$_3$-TPD desorption peak of H-ZSM-5, however, the high-temperature peak of the strong acid sites is observed to shift from 450°C to 700°C due to the generation of metal oxide nanoclusters after the introduction of copper, cerium and zirconium in the supported catalysts (Bin et al., 2014). Only one desorption peak located at approximately 200°C is clearly seen in the bulk-phase catalysts, as shown in Figure 4, which can be assigned to the physical adsorption of NH$_3$ (Wang et al., 2015).

Temperature-programmed desorption of oxygen

It was previously reported that the change in oxygen species over a catalyst follows $O_2 \rightarrow O_2^- \rightarrow O^- \rightarrow O^{2-}$ [4]. O_2, O_2^-/O^- and O^{2-} represent physically adsorbed oxygen, chemically adsorbed oxygen and lattice oxygen, respectively. The O_2-TPD profiles of the synthesized catalyst are displayed in Figure 5, and the corresponding O_2 adsorption content is provided in Table 3. Both adsorbed oxygen (α peak) and lattice oxygen (β peak) are detected in all catalyst samples. However, it is clearly

Figure 5. O_2-TPD profiles of $CuCe_{0.75}Zr_{0.25}O_y$ catalysts and $CuCe_{0.75}Zr_{0.25}O_y$/H-ZSM-5 catalysts.

Table 3. O_2-TPD data from $CuCe_{0.75}Zr_{0.25}O_y$ and $CuCe_{0.75}Zr_{0.25}O_y$/H-ZSM-5 catalysts.

Samples	α_1-O_2	α_2-O_2^-	α_3-O^-	β_1-O^{2-}	β_2-O^{2-}	Total
			O_2 adsorption ($\mu mol \cdot g^{-1}$)			
BP-gel	6	12	9	17	10	54
BP-td	5	17	8	10	10	50
BP-sr	6	9	4	6	9	34
S-si	11	10	6	5*		32
S-iwi	11	12	4	3*		30

*Represents lattice oxygen.

observed that the preparation method can greatly influence the amount of adsorbed oxygen and lattice oxygen.

Deconvolution of the broad α peak in Figure 5 produces three peaks (α_1, α_2 and α_3), where the α_1 peak is the O_2 desorption peak and the α_2 and α_3 peaks are the O_2^- and O^- desorption peaks, respectively (Luo et al., 2015, 2012). The β peak located at 600°C is attributed to the desorption of O^{2-} (Zhang et al., 2015b). The β_1 peak can be ascribed to the release of surface lattice oxygen, while the β_2 peak is attributed to the desorption of bulk lattice oxygen due to the decomposition of copper oxide into metallic copper (Moretti et al., 2013). However, obvious differences between the locations of the α and β peaks are clearly observed between the bulk-phase and the supported catalysts, especially the location of the β peak. The intense synergistic

effect between the active metal and support in the supported catalyst probably accounts for the shift in the β peaks.

It is accepted from Table 3 that the BP-gel catalyst possesses the largest amount of lattice oxygen species among all the catalysts tested, which suggests the production of more oxygen vacancies (Zhang et al., 2015b). The presence of the oxygen vacancies in the catalyst could greatly enhance the catalytic activity as verified by the following catalyst test (see 3.6 section).

Catalytic performance

The toluene conversion and CO_2 selectivity of the synthesized catalysts are shown in Figure 6, and the corresponding T_{10}, T_{50}, and T_{90} (temperature at which the VOC conversion is 10%, 50%, and 90%, respectively) values are listed in Table 4. It is clearly seen in Figure 6 that the catalytic activity is closely related to the preparation method, and the activities are in following order: BP-gel>S-si>S-iwi>BP-td>BP-sr. The degraded toluene can be completely converted into CO_2 and H_2O, while the CO_2 selectivity synchronously increases with an increase in the toluene conversion.

With respect to the bulk-phase catalyst, BP-gel exhibits the highest activity compared with the other two catalysts, and T_{10}, T_{50} and T_{90} are 137°C, 183°C and 219°C, respectively. At 260°C, toluene was almost completely degraded, which is 80°C lower than the temperature for the BP-td catalyst. For the BP-sr catalyst, the toluene
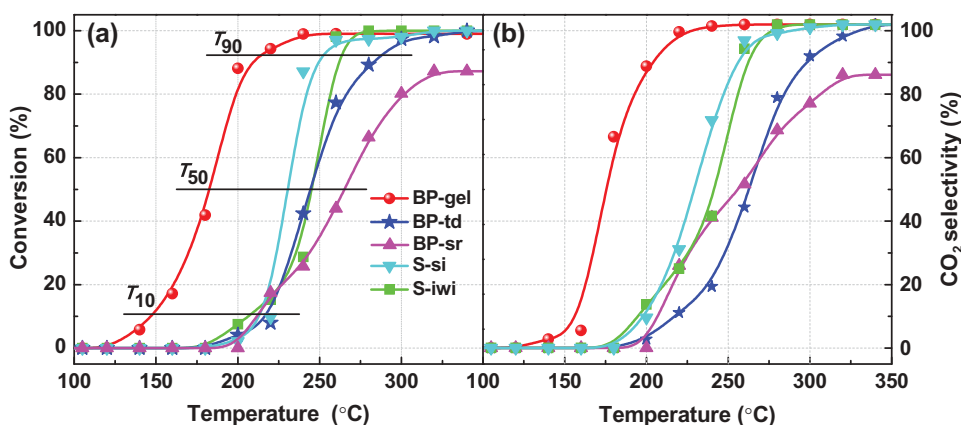
Figure 6. Toluene conversion (a) and CO_2 selectivity (b) over $CuCe_{0.75}Zr_{0.25}O_y$ and $CuCe_{0.75}Zr_{0.25}O_y$/H-ZSM-5 catalysts.

Table 4. T_{10}, T_{50} and T_{90} of $CuCe_{0.75}Zr_{0.25}O_y$ and $CuCe_{0.75}Zr_{0.25}O_y$/H-ZSM-5 catalysts for toluene catalytic oxidation.

Samples	T_{10} (°C)	T_{50} (°C)	T_{90} (°C)
BP-gel	137	183	219
BP-td	219	246	285
BP-sr	209	264	–
S-si	213	232	255
S-iwi	202	245	262

conversion was only 87.2%, although the temperature rose to 370°C. A close relationship between the activity and the properties of the bulk-phase catalysts was obtained. Both the reducibility and oxygen vacancies of the catalysts are crucial favorable factors for the catalytic degradation of VOCs, and in this case, the effect of the surface area on the bulk-phase catalytic activity could be ignored. The highest activity of the BP-gel catalyst can be explained as follows. First, the BP-gel catalyst possesses excellent reducibility and more active oxygen species. Second, according to the XRD and O_2-TPD results, the larger amount of oxygen vacancies presented in the BP-gel catalyst can promote the adsorption capacity of the Cu-Ce-Zr composite oxide catalysts for oxygen molecules (Delimaris & Ioannides, 2009), which improves the formation of reactive oxygen species. Therefore, the catalytic activities are highly consistent with the oxygen content (intensity of the β peaks) of the bulk-phase catalysts.
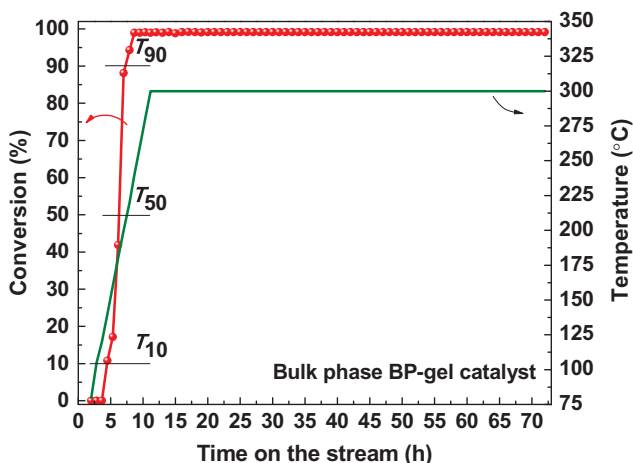
For the supported catalysts, the activity of S-si is slightly higher than that of the S-iwi catalyst. This should be ascribed to the fact that the S-si catalyst possesses larger amounts of finely dispersed CuO and lattice oxygen than the S-iwi sample. In addition, the larger surface area is also responsible for the higher activity of the S-si sample. The T_{50} and T_{90} of S-si are ca. 232°C and 255°C, respectively, which are 13°C and 7°C lower than those of S-iwi sample.

BP-gel exhibits a better catalytic performance than that of the S-si catalyst during the catalytic oxidation of toluene, not only owning to the excellent reducibility and oxygen vacancies but also to the larger pore structure properties. The pore size of the BP-gel sample, which has a mesoporous structure, is 6.52 nm, which is convenient for the migration and diffusion of toluene molecules (6.0 Å) (Bin et al., 2014). The prepared bulk-phase BP-gel only possesses fine mesopores, and the bulk-phase catalyst, with its porous structure, is more beneficial to the migration and diffusion of reactant molecules and further improves VOC degradation. In contrast, the microporous structure of S-si (0.53 nm) and S-iwi (0.37 nm) restricts the migration and diffusion of toluene and thus reduces the activity. The activity of the supported catalysts is higher than that of the BP-td catalyst. This may be attributed to the larger amount of bulk CuO in the BP-td sample, which decreases the synergetic effect between CuO and CeO_2 (Zou et al., 2009). For all the catalysts, no obvious relationships between the catalyst performances and the surface acidity were detected.

It is worth noting that the activity of the BP-gel catalyst toward toluene oxidation is superior to the reported catalysts. Moreover, the concentration of toluene in the present study is much higher than that reported in the literature (Deng et al., 2014), as displayed in Table 5. The T_{90} of the BP-gel catalyst is the lowest among the listed catalysts, which is only as low as 219°C. Researchers have explored other supports to improve the activity of catalysts. Tang et al. (Tang et al., 2004) used different morphologies of nano-CeO_2 as supports to prepare $La_{0.8}Ce_{0.2}MnO_3/CeO_2$ catalysts, and Lin et al. (Lin & Bai, 2016) synthesized hollow

Table 5. Comparison of catalytic performance for toluene destruction over various catalysts.

Samples	SV	Concentration (ppm)	T_{90} (°C)	Reference
$CuCe_{0.75}Zr_{0.25}O_y$	24,000 (h^{-1})	1500	219	This work
$Cu_{0.15}Ce_{0.85}O_x$	36,000 (h^{-1})	1000	231	He et al. (2014)
$Mn_{0.5}Ce_{0.5}$-HL	60,000 (ml·g/h)	1000	245	Tang et al., 2015
NiO-CTAB	20,000 (h^{-1})	1000	278	Bai et al. (2013)
0.3%Pd/ZSM-5	26,000 (h^{-1})	650	270	He et al. (2010)

Figure 7. Stability of the bulk phase BP-gel catalyst as a function of time on stream.

and mesoporous CoO_x/SiO_2 spheres as a supported catalyst. Although the activities of the $La_{0.8}Ce_{0.2}MnO_3/CeO_2$ and CoO_x/SiO_2 catalysts are higher than that of the S-si catalyst, the activities are lower than that of the BP-gel catalyst in this study, and T_{90} for $La_{0.8}Ce_{0.2}MnO_3/CeO_2$ was 240°C, which is higher than that of the BP-gel catalyst (219°C).

To evaluate the stability of the BP-gel catalyst, the reaction temperature for toluene oxidation was set at 300°C, since toluene was almost completely degraded over the bulk-phase BP-gel catalyst at 260°C (Figure 6). In Figure 7, the toluene conversion was almost maintained above 99% during testing for 72 h, and no deactivation was observed. The obtained result demonstrates that the stability of the BP-gel catalyst is excellent. The introduction of ZrO_2 in the bulk-phase catalyst should be responsible for such stability (Riva et al., 2009).

Conclusions

Different bulk-phase catalysts, $CuCe_{0.75}Zr_{0.25}O_y$, and supported catalysts, $CuCe_{0.75}Zr_{0.25}O_y/H$-ZSM-5, were successfully prepared, and the catalytic activities toward toluene oxidation were investigated in a fixed-bed reactor. The catalysts were comprehensively studied by BET, XRD, O_2-TPD, NH_3-TPD and H_2-TPR to elucidate their structural properties, reducibility and oxygen vacancies. The characterizations were also correlated to the catalytic performances to investigate the structure-property relationships. The results showed that the performance and structure of the Cu-Ce-Zr catalysts were closely associated with the preparation method. The bulk-phase BP-gel catalyst prepared by the sol-gel method exhibited the highest activity because its mesoporous structure with large mean pore sizes was beneficial for the mass transfer of reactant molecules and the convenient migration and diffusion of VOCs. In addition, the good low-temperature reducibility and rich oxygen vacancies of the BP-gel catalyst also enhanced the catalytic performances for toluene oxidation. Furthermore, the temperature of complete conversion was 260°C, and no deactivation phenomenon was observed during stability testing at 300°C for 72 h.

References

Bai, G.M., Dai, H.X., Deng, J.G., Liu, Y.X., Qiu, W.G., Zhao, Z.X., Li, X.W., and Yang, H.G. 2013. The microemulsion preparation and high catalytic performance of mesoporous NiO nanorods and nanocubes for toluene combustion. *Chem. Eng. J.*, **219**, 200–208.

Bin, F., Song, C.L., Lv, G., Song, J.O., Wu, S.H., and Li, X.D. 2014. Selective catalytic reduction of nitric oxide with ammonia over zirconium-doped copper/ZSM-5 catalysts. *Appl. Catal. B: Environ.*, **150–151**, 532–543.

Chen, H.H., Zhang, H.P., and Yan, Y. 2014. Fabrication of porous copper/manganese binary oxides modified ZSM-5 membrane catalyst and potential application in the removal of VOCs. *Chem. Eng. J.*, **254**, 133–142.

Delimaris, D., and Ioannides, T. 2009. VOC oxidation over CuO-CeO_2 catalysts prepared by a combustion method. *Appl. Catal. B: Environ.*, **89**, 295–302.

Deng, Q.F., Ren, T.Z., Agula, B., Liu, Y.P., and Yuan, Z.Y. 2014. Mesoporous $CexZr_{1-x}O_2$ solid solutions supported CuO nanocatalysts for toluene total oxidation. *J. Ind. Eng. Chem.*, **20**, 3303–3312.

Dou, B.J., Hu, Q., Li, J.J., Qiao, S.Z., and Hao, Z.P. 2011. Adsorption performance of VOCs in ordered mesoporous silicas with different pore structures and surface chemistry. *J. Hazard. Mater.*, **186**, 1615–1624.

Ge, T.G., Hua, Z.L., He, X.Y., Zhu, Y., Ren, W.C., Chen, L.S., Zhang, L.X., Chen, H.G., Liu, C.C., Yao, H.L., and Shi, J.L. 2015. One-pot synthesis of hierarchically structured ZSM-5 zeolites using single micropore-template. *Chin. J. Catal*, **36**, 866–873.

Gutiérrez-Ortiz, J.I., Rivas, B.D., López-Fonseca, R., and González-Velasco, J.R. 2006. Catalytic purification of waste gases containing VOC mixtures with Ce/Zr solid solutions. *Appl. Catal. B: Environ.*, **65**, 191–200.

He, C., Li, P., Cheng, J., Hao, Z.P., and Xu, Z.P. 2010. A comprehensive study of deep catalytic oxidation of benzene, toluene, ethyl acetate, and their mixtures over Pd/ZSM-5 catalyst: mutual effects and kinetics. *Water Air Soil Pollut.*, **209**, 365–376.

He, C., Xu, B.T., Shi, J.W., Qiao, N.L., Hao, Z.P., and Zhao, J.L. 2015a. Catalytic destruction of chlorobenzene over mesoporous $ACeO_x$ (A = Co, Cu, Fe, Mn, or Zr) composites prepared by inorganic metal precursor spontaneous precipitation. *Fuel Process. Tech.*, **130**, 179–187.

He, C., Yu, Y.K., Shi, J.W., Shen, Q., Chen, J.S., and Liu, H.X. 2015b. Mesostructured Cu–mn–Ce–O composites with homogeneous bulk composition for chlorobenzene removal: Catalytic performance and microactivation course. *Mater. Chem. Phys.*, **157**, 87–100.

He, C., Yu, Y.K., Yue, L., Qiao, N.L., Li, J.J., Shen, Q., Yu, W.J., Chen, J.S., and Hao, Z.P. 2014. Low-temperature removal of toluene and propanal over highly active mesoporous $CuCeO_x$ catalysts synthesized via a simple self-precipitation protocol. *Appl. Catal. B: Environ.*, **147**, 156–166.

Hu, C.Q., Zhu, Q.S., and Jiang, Z. 2009. Nanosized CuO–$zr_xCe_{1-x}O_y$ aerogel catalysts prepared by ethanol supercritical drying for catalytic deep oxidation of benzene. *Powder Tech.*, **194**, 109–114.

Jia, A.P., Hu, G.S., Meng, L., Xie, Y.L., Lu, J.Q., and Luo, M.F. 2012. CO oxidation over $CuO/Ce_{1-x}Cu_xO_{2-\delta}$ and $Ce_{1-x}Cu_xO_{2-\delta}$ catalysts: synergetic effects and kinetic study. *J. Catal*, **289**, 199–209.

Kuo, C.P., Liao, H.T., Chou, C.C.K., and Wu, C.F. 2014. Source apportionment of particulate matter and selected volatile organic compounds with multiple time resolution data. *Sci. Total. Environ.*, **472**, 880–887.

Li, S.M., Hao, Q.L., Zhao, R.Z., Liu, D.L., Duan, H.Z., and Dou, B.J. 2016. Highly efficient catalytic removal of ethyl acetate over Ce/Zr promoted copper/ZSM-5 catalysts. *Chem. Eng. J.*, **285**, 536–543.

Lin, L.Y. and Bai, H.L. 2016. Salt-induced formation of hollow and mesoporous CoOx/SiO2 spheres and their catalytic behavior in toluene oxidation. *RSC Adv*, **6**, 24304–24313.

Lu, H.F., Kong, X.X., Huang, H.F., Zhou, Y., and Chen, Y.F. 2015. Cu–mn–ce ternary mixed-oxide catalysts for catalytic combustion of toluene. *J. Environ. Sci.*, **32**, 102–107.

Luo, J.J., Xua, H.Y., Liu, Y.F., Chu, W., Jiang, C.F., and Zhao, X.S. 2012. A facile approach for the preparation of biomorphic CuO-ZrO2 catalyst for catalytic combustion of methane. *Appl. Catal. A: Gen.*, **423–424**, 121–129.

Luo, M.F., Ma, J.M., Lu, J.Q., Song, Y.P., and Wang, Y.J. 2007. High-surface area CuO–ceO2 catalysts prepared by a surfactant-templated method for low-temperature CO oxidation. *J. Catal*, **246**, 52–59.

Luo, Y.J., Qian, Q.R., and Chen, Q.H. 2015. On the promoting effect of the addition of $Ce_xZr_{1-x}O_2$ to palladium based alumina catalysts for methanol deep oxidation. *Mater. Res. Bull.*, **36**, 866–873.

Moretti, E., Lenarda, M., Riello, P., Storaro, L., Talon, A., and Frattini, R. 2013. Influence of synthesis parameters on the performance of CeO_2-CuO and CeO_2-ZrO_2-CuO systems in the catalytic oxidation of CO in excess of hydrogen. *Appl. Catal. B: Environ.*, **129**, 556–565.

Moretti, E., Molina, A.I., Sponchia, G., Talon, A., Frattini, R., Rodriguez-Castellon, E., and Storaro, L. 2017. Low-temperature carbon monoxide oxidation over zirconia-supported CuO-CeO2 catalysts: effect of zirconia support properties. *Appl. Surf. Sci.*, **403**, 612–622.

Riva, B.D., Pez-Fonseca, R.L., Sampedro, C., and Gutiérrez-Ortiz, J.I. 2009. Catalytic behaviour of thermally aged Ce/Zr mixed oxides for the purification of chlorinated VOC-containing gas streams. *Appl. Catal. B: Environ.*, **90**, 545–555.

Tang, W.X., Li, W.H., Shan, X., Wu, X.F., and Chen, Y.F. 2015a. Template-free synthesis of hierarchical layer-stacking CeO_2 nanostructure with enhanced catalytic oxidation activity. *Mater. Lett.*, **140**, 95–98.

Tang, W.X., Wu, X.F., Liu, G., Li, S.D., Li, D.Y., Li, W.H., and Chen, Y.F. 2015b. Preparation of hierarchical layer-stacking Mn-Ce composite oxide for catalytic total oxidation of VOCs. *J. Rare Earth*, **33**, 62–69.

Tang, X.L., Zhang, B.C., Li, Y., Xu, Y.D., Xin, Q., and Shen, W.J. 2004. Carbon monoxide oxidation over CuO/CeO2 catalysts. *Catal. Today*, **93–95**, 191–198.

Wang, J., Yunus, R., Li, J., Li, P., Zhang, P., and Kim, J. 2015a. In situ synthesis of manganeseoxides on polyester fiber for formaldehyde decomposition at room temperature. *Appl. Surf. Sci.*, **357**, 787–794.

Wang, Z., Qu, Z.P., and Fan, R. 2015b. The Al promotional effect for $Ce_{0.4}Zr_{0.6}O_2$ mixed oxides in selective catalytic oxidation of ammonia to nitrogen. *Sep. Purif. Tech.*, **147**, 24–31.

Zhang, L.F., He, Y.C., Yang, X.J., Yuan, H., Du, Z.P., and Wu, Y.X. 2015a. Oxidative carbonylation of phenol to diphenyl carbonate by Pd/MO-MnFe2O4 magnetic catalyst. *Chem. Eng. J.*, **278**, 129–133.

Zhang, Q.L., Xu, L.S., Ning, P., Gu, J.J., and Guan, Q.Q. 2014. Surface characterization studies of CuO-CeO2-ZrO2 catalysts for selective catalytic reduction of NO with NH_3. *Appl. Surf. Sci.*, **317**, 955–961.

Zhang, Z.X., Jiang, Z., and Shangguan, W.F. 2015b. Low-temperature catalysis for VOCs removal in technology and application: a state-of-the-art review. *Catal. Today*, **264**, 270–278.

Zhou, G.L., Lan, H., Gao, T.T., and Xie, H.M. 2014. Influence of Ce/Cu ratio on the performance of ordered mesoporous CeCu composite oxide catalysts. *Chem. Eng. J.*, **246**, 53–63.

Zou, Z.Q., Meng, M., Zha, Y.Q., Zou, Z.Q., Meng, M., and Zha, Y.Q. 2009. The effect of dopant Cu, Fe, Ni or La on the structures and properties of mesoporous Co-Ce-O compound catalysts. *J. Alloy. Compd.*, **470**, 96–106.